NASA CONTRACTOR REPORT

NASA CR-2668

FABRICATION AND SURFACE CHARACTERIZATION OF COMPOSITE REFRACTORY COMPOUNDS SUITABLE FOR THERMIONIC CONVERTERS

L. W. Swanson, J. T. Dickinson, and D. R. McNeely

Prepared by
OREGON GRADUATE CENTER
Beaverton, Oreg. 97005
for Lewis Research Center

NATIONAL AERONAUTICS AND SPACE ADMINISTRATION • WASHINGTON, D. C. • APRIL 1976

1. Report No.	2. Government Accession No.	3. Recipient's Ca.
NASA CR-2668		

4. Title and Subtitle	5. Report Date
FABRICATION AND SURFACE CHARACTERIZATION OF COMPOSITE REFRACTORY COMPOUNDS SUITABLE FOR THERMIONIC CONVERTERS	March 1976
	6. Performing Organization Code
7. Author(s)	8. Performing Organization Report No.
L. W. Swanson, J. T. Dickinson, and D. R. McNeely	None
	10. Work Unit No.
9. Performing Organization Name and Address	
Oregon Graduate Center 19600 N. W. Walker Road Beaverton, Oregon 97005	11. Contract or Grant No. NSG-3054
	13. Type of Report and Period Covered
12. Sponsoring Agency Name and Address	Contractor Report
National Aeronautics and Space Administration Washington, D. C. 20546	14. Sponsoring Agency Code

15. Supplementary Notes

Topical Report. Project Manager, James F. Morris, Physical Science Division, NASA Lewis Research Center, Cleveland, Ohio

16. Abstract

Procedures for fabricating high purity single crystals of LaB_6 and SmB_6 have been developed. Auger spectroscopy shows that a clean surface can be obtained by thermal heating at 1700 K; such a clean surface gives a value of B/La of 2.3 to 2.6 for the (100) face. The measured thermionic and FERP work functions of the (100) face of LaB_6 are 2.47 and 2.28 eV, respectively. The electron reflection coefficient for LaB_6(100) increases near zero primary energy to 0.5. Flash thermal desorption of an oxygen dosed surface showed that B_2O_3 is the desorption product at 1600 to 1700 K. A work function increase of 1.6 eV was observed on oxygen adsorption on LaB_6(100). Thermal desorption of Co occurs at ~1300 K. A reduction of the work function to 1.39 eV was observed on adsorption of a partial monolayer of Cs on LaB_6(100). The evaporation of LaB_6 occurs as atomic La and B with a value of B/La of 6 to 3 in the temperature range 1700 to 2000 K. The activation energies of desorption for La and B are 6.3 ± 0.3 and 6.8 ± 0.3 eV, respectively

17. Key Words (Suggested by Author(s))	18. Distribution Statement
Thermionic conversion; Electron emission; Electron reception; Metallides; Single crystals; Thermophysicochemical characteristics	Unclassified - unlimited STAR Category 70 (rev.)

19. Security Classif. (of this report)	20. Security Classif. (of this page)	21. No. of Pages	22. Price*
Unclassified	Unclassified	39	$3.75

* For sale by the National Technical Information Service, Springfield, Virginia 22161

Table of Contents

I. INTRODUCTION

The direct conversion of heat to electricity with a reasonable degree of efficiency and simplicity has been the primary objective of those involved in thermionic converter technology for the past decade. A cesium gas filled diode operating at relatively high pressures appears to be the most promising of the various embodiments tested to date. Unfortunately, efficiencies seldom exceed 10% and practical power outputs are $\sim$ 5 to 10 watts/cm^2 at 1700K to 2000K.

It is believed that the use of low work function electrode materials such as lanthanum hexaboride (LaB_6) may increase efficiencies by a factor of 3 and result in power outputs between 15 and 40 watts/cm^2 at 1700 K.[1] Other metal boride compounds such as YB_6, SmB_6, TaB_2, and W_2B_2 also look promising as electrode materials. Unfortunately, surface properties and fabrication techniques of the metal borides need considerably more elucidation before an informed assessment of the anticipated improvement in operating parameters of thermionic converters can be made.

The primary objective of this research program is to establish reliable techniques of materials fabrication and to gain understanding of the basic surface properties relating to thermionic converter performance of the above mentioned materials. Particular attention is being devoted to the fabrication of ultra pure, single crystal materials on which techniques of Auger spectroscopy, low energy electron diffraction and field electron and ion microscopy can be employed. In addition to the analysis of surface composition and structure of the clean surfaces, a further objective of this program has been the measurement of the kinetics and energetics of cesium adsorption/desorption. Also, considerable study is being given to the work function and

electron reflection measurements of clean and cesiated surfaces.

This report is a description of the progress made during the first six months of this program. It is convenient to categorize the research effort into the following tasks:

I. Materials Development

II. Clean Surface Characterization

III. Cesiated Surface Characterization

Under the "Clean Surface Characterization" task we are examining the following:

1. Surface work function
2. Surface composition
3. Surface geometric structure
4. Electron reflection coefficient
5. Thermal stability of the surface
6. Gas adsorption

With respect to Task III, Cesiated Surface Characterization, we are carrying out the following measurements on the various materials:

1. Work function/cesium coverage relationships
2. Cesium coverage/temperature relationship
3. Cesium thermal desorption kinetics
4. Electron reflection coefficient of cesiated surfaces
5. Cesium and oxygen co-adsorption

II. Material Fabrication and Selection

The philosophy of approach to material fabrication in this study is to employ methods that will provide the highest purity single crystal specimens possible. Much of the previous studies of the surface properties of the metal

boride compounds have been hampered by unknown concentrations of bulk impurities segregated at the surface and by the use of polycrystalline specimens which hinder analysis of the anisotropy of surface properties with crystallographic orientation.

The rare earth boride compounds we selected for investigation were those expected to exhibit a low work function surface and suitable for single crystal fabrication. From Table I it is noted that the RB_6 rare earth compounds which form congruently (as opposed to peritecticly) are between La and Eu. If we assume that a low value of ionization potential for the rare earth element leads to a lower value of surface work function, La, Sm and Eu stand out as likely candidates as low work function RB_6 compounds. Lattice constants of the RB_6 compounds are remarkably independent of the rare earth element as seen from Table I. To date single crystal material fabrication has been limited to the rare earth hexaborides.

A new era of metal-boride single crystal fabrication began with the discovery of various single crystal shapes precipitating from liquid aluminum.[3] The method consists of mixing stoichiometrically the basic elements of the boride compound, e.g. powdered B and metallic rare earth metal, in an inert crucible and heating in an argon atmosphere to ~ 1500°C. After cooling the solid Al solvent was dissolved with warm HCl leaving needle and plate-like single crystals of the boride compound. The details of the fabrication procedures and results for La and Sm hexaboride are given below.

1. Experimental Procedures

The first molten metal flux precipitation of single crystals was performed by P. Lebeau and J. Eiguras[4] and is referred to as the "Lebeau" or "molten flux" method of single crystal growth. The starting materials in our application of this method consisted of 60 mesh boron powder, ingot formed aluminum, and metallic chips of lanthanum and samarium. Table II lists

TABLE I

Summary of Rare Earth Properties

Element	First Ioniz. Pot. (eV)	Second Ioniz. Pot. (eV)	RB_6*	RB_4*	Lattice Constant[2] (A)	RB_6 M.P.(C)
Y	6.38	12.23	P	P	4.113	2600
Ba	5.21	10.00			4.268	2270
La	5.61	11.43	C	P	4.157	2715
Ce	6.54	12.31	C	P	4.141	2550
Pr	5.76		C	P	4.130	2610
Nd	6.31		C	P	4.128	2610
Sm	5.60	11.4	C	P	4.129	2580
Eu	5.67	11.24	C		4.178	2580
Gd	6.16	12.0	P	C	4.110	2510
Tb	6.74		P	C		
Dy	6.82		P	C		
Ho			P	C		
Er	6.08		P	C	4.11	
Tm	5.81		P	C		
Yb	6.22	12.1	C	P	4.14	
Lu	6.15	14.7		C		

P - peritectic

C - congruent

typical impurity levels for the starting materials used in the single crystal preparation.

TABLE II

Bulk Purity Specifications of the Various Materials

Measured by Optical Emission Spectrographic Techniques

Material	Impurities (ppm)											
	Si	Mg	Fe	Cu	Al	Ca	Ni	O	C	Ag	Eu	Nd
Aluminum	3	<1	2	1	<1	<1	<1	-	<1	<1	-	-
Lanthanum	300	-	300	-	300	500	300	-	-	-	-	-
Boron	<20	<20	250	<20	<20	<20	<20	100	300	-	-	-
Samarium	<100	-	100	<100	<100	<100	-	-	-	-	500	300
LaB_6*	100	100	<10	<10	-	100	<10	-	-	100	-	-

*single crystals prepared

The LaB_6 single crystal growths were performed in 30 ml alumina boats placed in a resistively heated silicon carbide globar horizontal tube furnace. The boron was placed in four 4.8 mm diameter holes bored in the aluminum ingot and the lanthanum was placed on the top center of the ingot. Before each run the growth chamber was evacuated and backfilled to one atmosphere pressure with high purity argon. The heating rate was from room temperature to 1500° C over a period of 6 hours and maintained at 1500° C for 8 hours. Cooling from 1500° C to 800° C took place at the conductive cooling rate of the furnace over a period of 1.5 hours; further cooling to room temperature occurred conductively over a 2 hour period.

After dissolving the Al solvent with HCl large single crystal platelets (approximately 2 mm square by 0.1 mm and some 1 x 7 x 0.1 mm) formed. Cubic

shapes also 1 to 2 mm on a side were also observed. In addition, needle shapes 6 to 8 mm long and 0.1 to 0.2 mm square cross section were produced. A typical selection of these crystal shapes are shown in Fig. 1. Similar results, shown in Fig. 1, were obtained with Sm.

2. Material Evaluation

Optical emission spectrographic analysis of the prepared LaB_6 single crystals indicated, according to the Table II summary, that crystal purity was superior to the starting materials. Subsequent surface analysis of the crystals after flashing the ~ 1600 K showed only La and B. Apparently even the Al solvent is not incorporated into the growing crystals of LaB_6.

Among the platelet shaped crystals could be found many that exhibited unusually smooth surfaces. No ledges or surface imperfections could be detected by SEM inspection at 50 K times for several of these crystals.

X-ray diffraction pictures of the platelet surface shown in Fig. 2 indicate a (100) direction perpendicular to the platelet face. Likewise, x-ray diffraction of the longitudinal faces of the needle structures gave (100) faces as shown in Fig. 2. Thus the needle axis, which is the growth direction, is a (100) direction. The sharpness of the x-ray diffraction spots indicate relatively defect free single crystal specimens.

From powder x-ray diffraction patterns a lattice constant for the LaB_6 crystals of 4.156 Å was obtained; this is in excellent agreement with the literature value of 4.157 Å given in Table I. Similar x-ray examination of the prepared SmB_6 crystals gave a lattice constant of 4.132 Å also in good agreement with the Table I literature value of 4.129 Å.[2]

In summary, we conclude that the liquid metal flux technique of forming small single crystals of LaB_6 and SmB_6 is successful. The crystals,

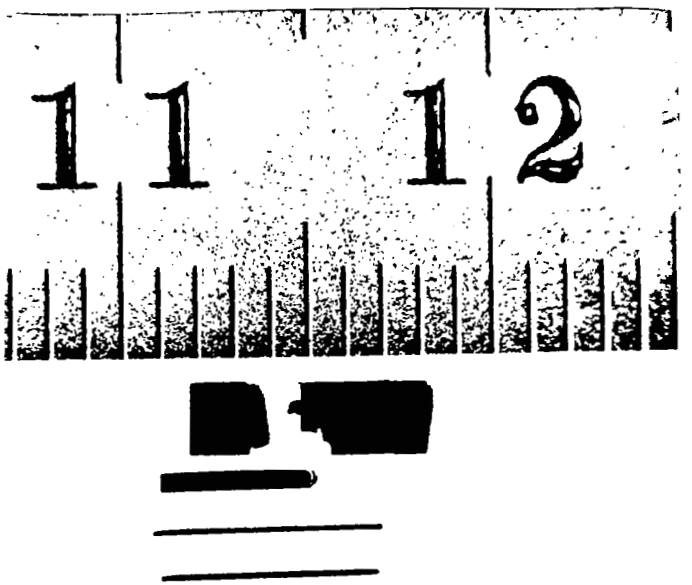

SmB_6 Size

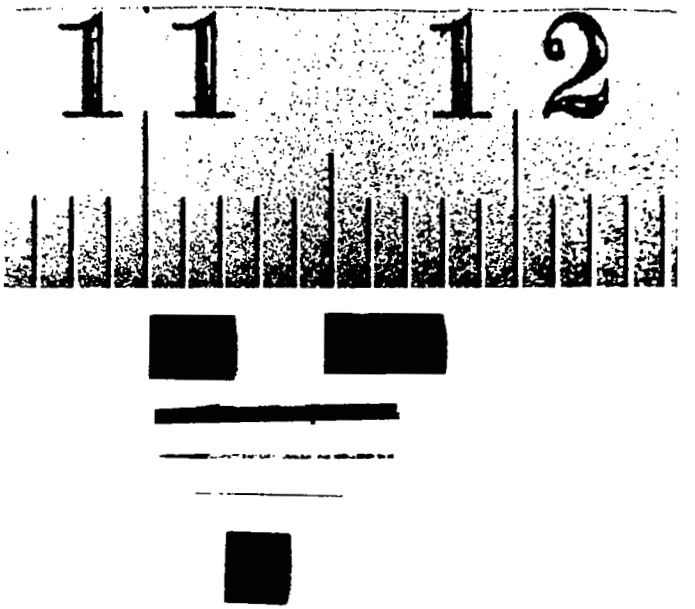

LaB_6 Size

Figure 1. Typical shapes and sizes of the LaB_6 and SmB_6 single crystals produced by the liquid aluminum flux technique.

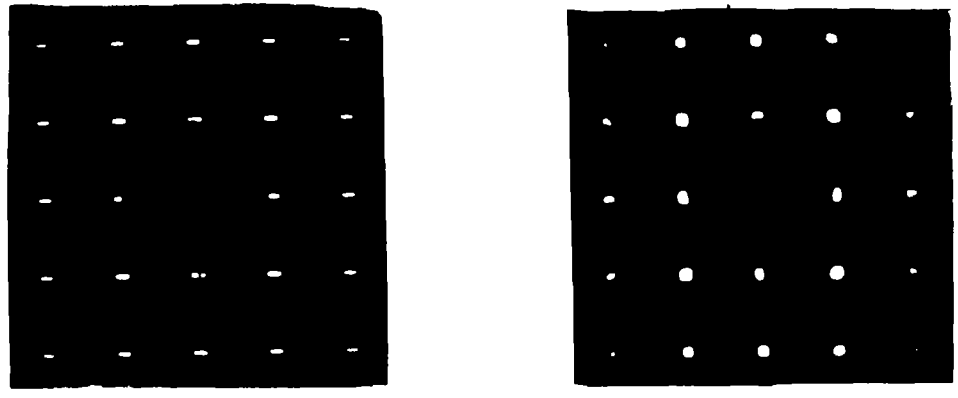

(a) (b)

Figure 2. X-ray diffraction patterns of (a) the longitudinal face of a LaB_6 needle shape crystal and (b) the face of a LaB_6 single crystal platelet.

which develop (100) faces, are both extremely pure and defect free. It is our expectation that all the rare earth hexaboride compounds that, according to Table I, exhibit congruently melting hexaborides will form single crystals by this technique. Interestingly, no evidence of the peritecticly formed tetraboride structures was observed in our preparations of LaB_6 and SmB_6.

III. Clean Surface Characterization

Our surface characterization results to date are confined to the (100) crystal face of LaB_6. Four techniques employed to characterize the crystal surface properties are 1) Auger electron spectroscopy (AES) measurement of surface composition; 2) mass spectroscopic measurement of desorbing species; 3) field emission retarding potential (FERP) technique for low temperature work function measurement and reflection coefficients; and 4) thermionic emission measurement of high temperature work function.

1. Experimental Procedures

Most of the surface studies have been performed in an Ultec TBK 250 ℓ/sec vac-ion pumped vacuum chamber. A Physical Electronics Corp. cylindrical mirror electron energy analyzer used for AES was mounted in the specimen chamber. Mounted opposite to the AES was an EAI Corp. Model 160 quadrupole spectrometer used for measuring the mass spectrum of desorbing species from the specimen surface. An ion gun was mounted so as to allow simultaneous ion sputtering and Auger analysis of the specimen. Mounted between the 4" diameter viewing port and the AES was a FERP gun which was used to measure the room temperature work function of the specimen. The FERP method, which is described elsewhere,[5] involves measuring the retarding potential I(V) characteristics on the specimen using a field emitter as the electron source. It has been shown that the absolute (as opposed to relative) work function of the collector surface is measured by this method. In addition,

the electron reflection coefficient as a function of primary beam energy can be measured by the FERP technique.[5] The size of the analyzing electron beams for the FERP and AES measurements was 0.8 and .03 mm respectively.

The study of the adsorption of various gases on the crystal specimens was accomplished by inletting the gas through a Varian leak valve connected to a separately pumped gas inlet system. The purity of the research grade gases used in this study exceeded 4N and was monitored by the mass spectrometer during adsorption.

The LaB_6 platelets were mounted on a tantalum sheet which was first coated with a thin layer of carbon (aquadag). While the coating of carbon was still moist the crystal was pressed on and heated slowly up to a dull red color. The heating was accomplished by indirect heating of the Ta support with a tungsten filament. Temperature measurements were made pyrometrically using an emissivity correction of 0.8[6] and by a W/25% Re thermocouple spot welded to the Ta support.

For field electron microscope (FEM) studies the needle shaped crystals were mechanically held between two Re .001" sheets that could be heated resistively. Sharp points suited for FEM studies were formed on the ends of the needles by electrochemical etching in 50% NaOCl/methanol solution using 2 V dc.

It should be stated that historically the methods of mounting LaB_6 on a support suitable for heating have not proven to be totally successful. The problems are 1) excessive diffusion of B into the substrate at high temperature, and 2) mismatch of thermal expansion coefficients. Re has generally been found to be the most suitable support that eliminates B diffusion. We found that Re was a thermally stable support for LaB_6 but the crystal must be mechanically held to the Re since the diffusion bonding was not adequate.

The carbon film on Ta also provided an adequate bond although on occasion the carbon film peeled off the Ta substrate.

2. LaB_6 Surface Cleaning

As mentioned previously the bulk purity of the LaB_6 crystals was very high, thus we were hopeful that thermal cleaning of the surface would be adequate. Use of AES to monitor the LaB_6 surface showed mainly O, C, N, and small concentrations of Al present during thermal cleaning. The C usually was present as CO or CO_2 which could be removed by heating at 1200 to 1300 K. The most tenaciously bound impurity was O which could be removed by heating at 1600 to 1700 K. Thus, we were able to routinely obtain clean surface conditions by flashing the crystal to ~ 1700 K.

Fig. 3 shows the variation of AES signal strength (in atomic %, using the pure element sensitivity factors given by the manufacturer, Physical Electronics Corp.) with crystal temperature after exposure to 3×10^{-6} torr-sec of O_2. Only B, La, O and a small amount of C were observed on the surface. Notice that O is completely removed at ~1600K. Simultaneous with the removal of O is an increase in the B signal strength while the La signal level remains virtually unchanged. Based on the sensitivity factors used in this study, which are listed in Table III, the ratio of B/La observed for a thermally clean surface was 2.3 to 2.6.

3. Oxygen Adsorption and Desorption on LaB_6 (100)

Fig. 4 shows an AES spectrum of the (100) crystal face of LaB_6 before and after exposure to 3.0×10^{-6} torr sec. of O_2. The presence of the chemisorbed O_2 layer caused a reduction in the B/La ratio to ~ 1.3 and accentuated the doublet feature in the 625 eV $La(M_{IV,V}N_{IV,V}N_{IV,V})$ transition. Shown in Fig. 5 are the variations of the room temperature work function ϕ (as measured by the FERP technique) and O(510) AES signal strength with O_2

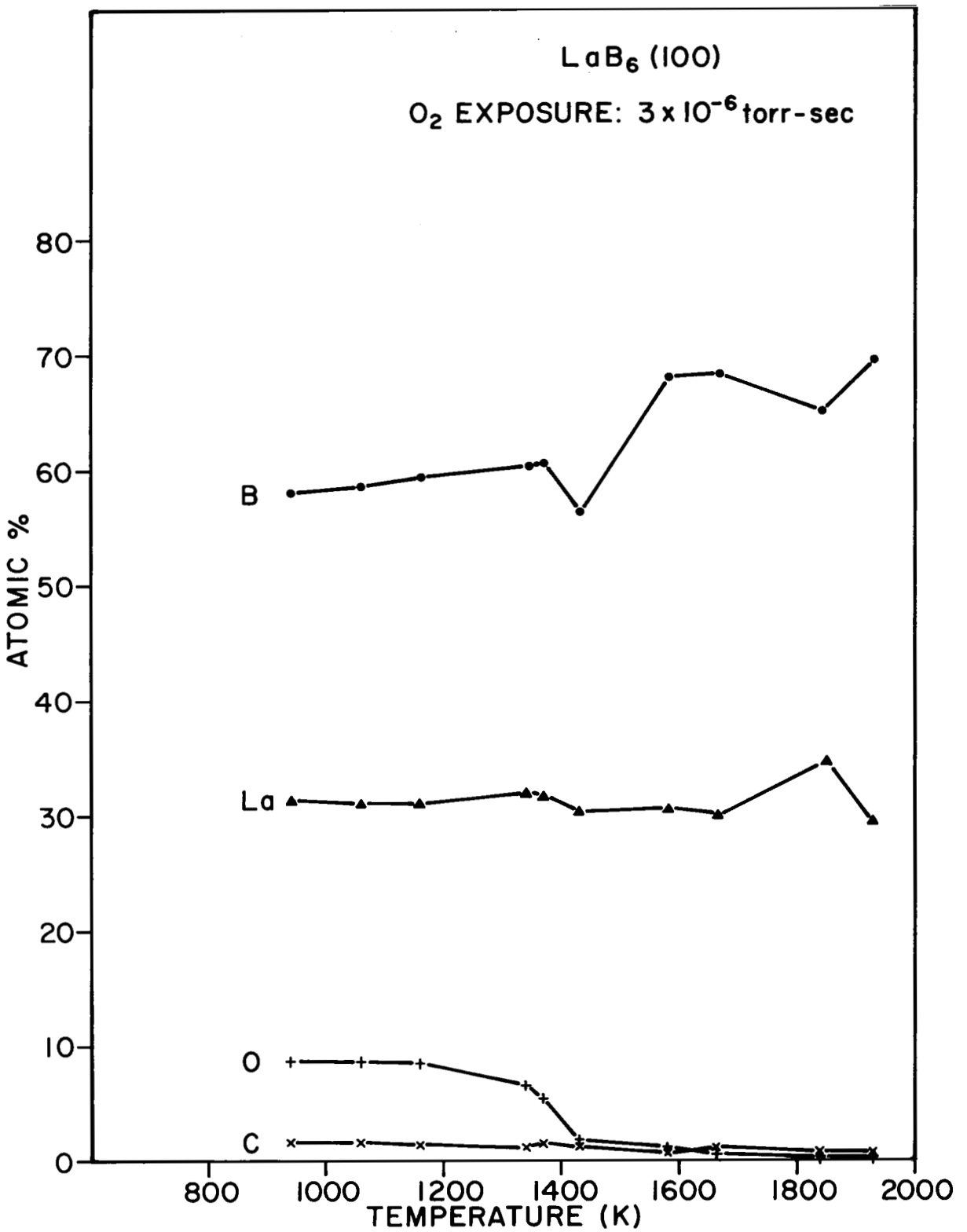

Figure 3 Variation of the Auger signal strength (in atomic percent) with temperature for the various elements observed on a LaB_6(100) crystal face after exposure to pure oxygen at room temperature.

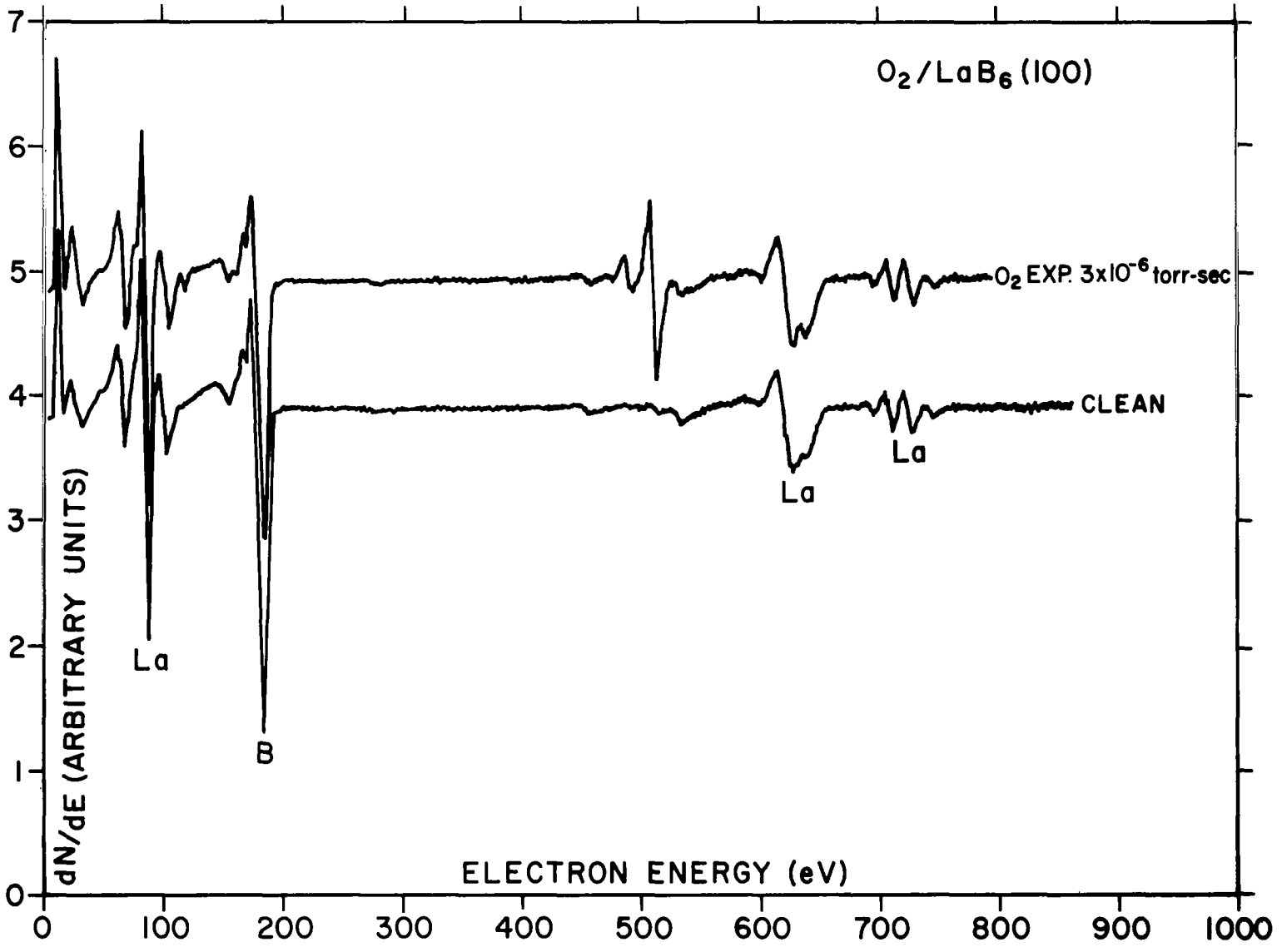

Figure 4 Auger derivative spectrum of a clean and oxygen covered LaB_6(100) crystal face using 2 V modulating voltage. Electron gun conditions: V = 4 kV and I = 10 μA.

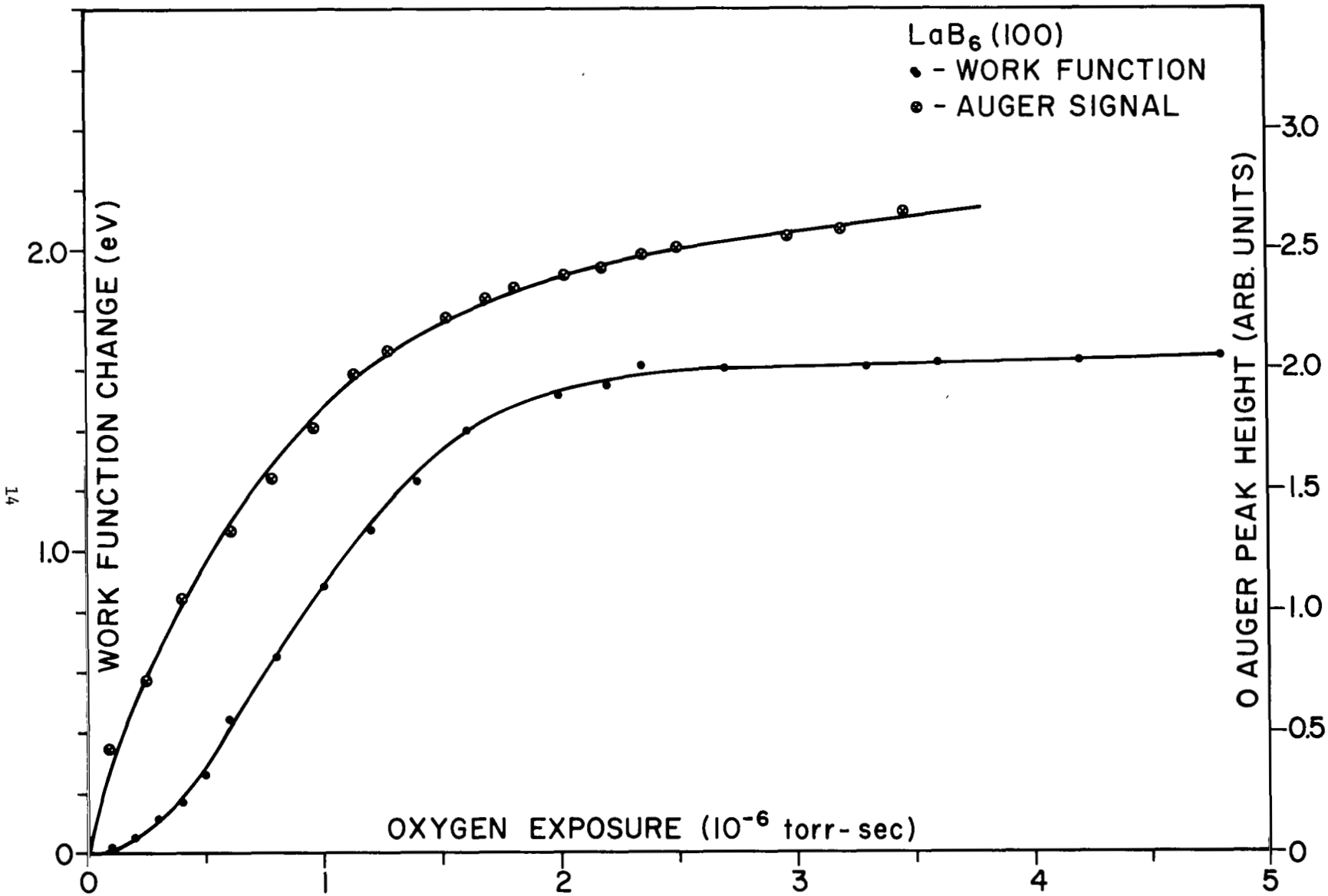

Figure 5 Curves show the variation of the FERP work function and oxygen 510 eV Auger signal strength versus oxygen exposure for a LaB_6(100) crystal face. T = 300 K.

Table III

AES Relative Sensitivities Used in this Study

Normalized to Unity for Pure Ag

Element (AES Energy)	Sensitivity
B (179)	0.138
C (271)	0.111
N (381)	0.365
O (510)	1.02
Al (1396)	0.049
Cs (563)	0.097
La (625)	0.075

exposure. If one assumes that the O (510) AES signal varies linearly with O coverage, then the variation of work function $\Delta\phi$ with O relative coverage θ can be obtained as shown in Fig. 6. Of particular interest in Fig. 6 is the increasing value of $d\phi/d\theta$ almost to the saturation value of $\Delta\phi$ = 1.6 eV arbitrarily chosen as θ = 1.

Next, we consider the thermal desorption kinetics of the chemisorbed O. Much to our surprise we found, by use of the quadrupole mass spectrometer to measure the desorbing species, that only a mass 70 product was thermally desorbed after O_2 adsorption. A typical flash desorption spectra of the mass 70 desorption product is shown in Fig. 7 where 2.4 x 10^{-6} torr-sec. of O_2 was adsorbed at increasing value of the substrate temperature. We concluded that the desorbing species was B_2O_3. An AES signal strength for O (510) vs temperature for room temperature adsorption is also shown in Fig. 7. The increase in the mass 70 peak for T > 1800 K is due to the La^{++} peak

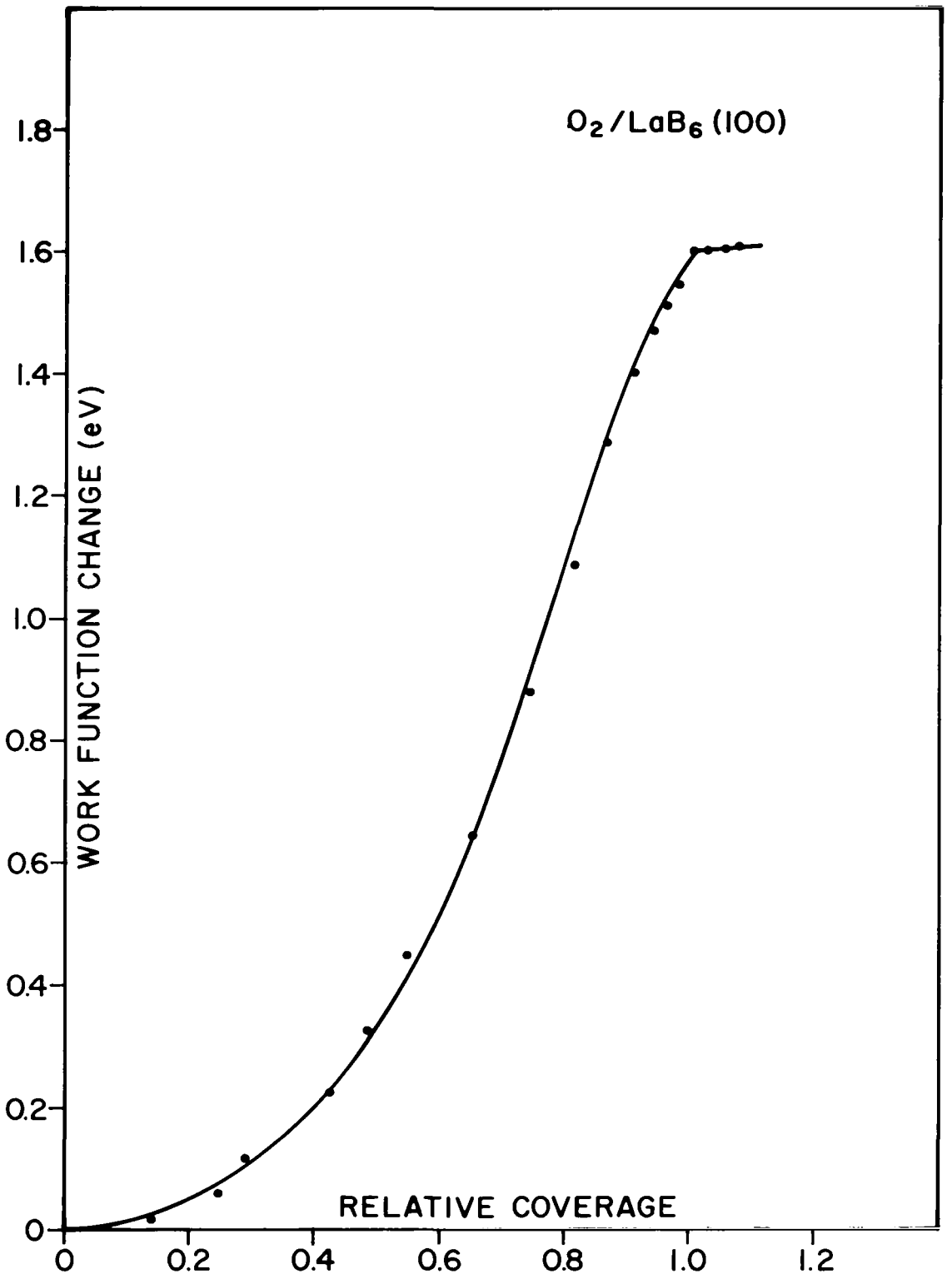

Figure 6 Curve shows the FERP work function variation with relative oxygen coverage for a LaB_6(100) crystal at room temperature. Coverage scale based on Figure 5 Auger signal strength.

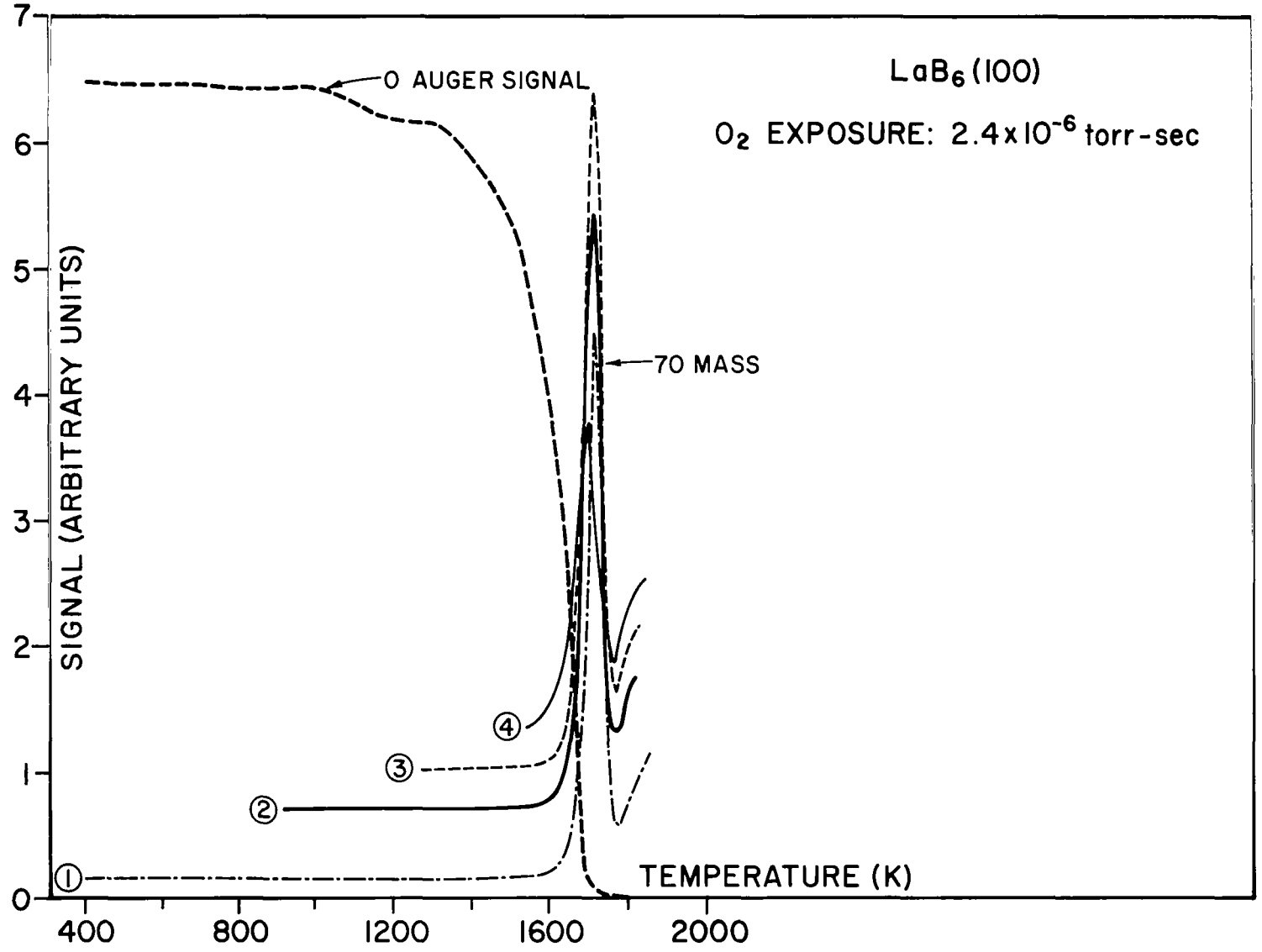

Figure 7 Curves show the variation of the O (510) Auger and mass 70 signal strength with increasing temperature of an oxygen covered LaB_6(100) crystal face. Curves 1 through 4 indicate that the oxygen exposure of 2.4×10^{-6} torr-sec was carried out with the crystal at the indicated temperature. The heating rate was ~15 K/sec.

which overlaps the mass 70 peak and begins to occur above 1800 K.

Upon close examination we found that adsorption of an equal sized dose of O_2 gave an equal sized (in terms of area under the curve) mass 70 desorption peak unless the substrate temperature during adsorption exceeded ~ 1400 K. Variation of the dose size at room temperature produced no change in the temperature of the peak maximum in Fig. 7. This interesting and unusual result means that the sticking probability and reaction efficiency to form B_2O_3 is unchanged for $T < 1400$ K.

4. CO Adsorption and Desorption on LaB_6 (100)

Preliminary Auger and mass spectrometer investigations of CO adsorption and desorption have been carried out. Fig. 8 shows a clean and CO covered Auger spectrum for LaB_6 (100). In contrast to O adsorption, CO does not cause a shape change in the La (625 eV) peak. On the other hand, as shown in the expanded C (271 eV) peak in Fig. 8, a slight modification of the high energy side of the C (271 eV) peak was observed.

Using the Table III sensitivities we show in Fig. 9 the variation in atomic percent of the surface composition upon CO adsorption. The ratio of C/O = 1.4 to 1.6 and the La atomic percent are relatively constant with CO coverage. Like the O adsorption, Fig. 9 shows that the B Auger signal strength is reduced by the presence of CO.

Fig. 10 shows the variation of the O (510 eV) Auger signal strength with CO adsorption at 300 K. A comparison with Fig. 5 shows that *both O_2 and CO saturate the Auger signal strength at an exposure between* 2 to 3 x 10^{-6} torr-sec.

Only very preliminary study of the desorption of CO has been carried out. Fig. 11 shows the variation of the 28 mass, and C (271) and O (510) Auger signal strengths with substrate temperature after a monolayer adsorption of CO. Because of the simultaneous change of the Auger signal

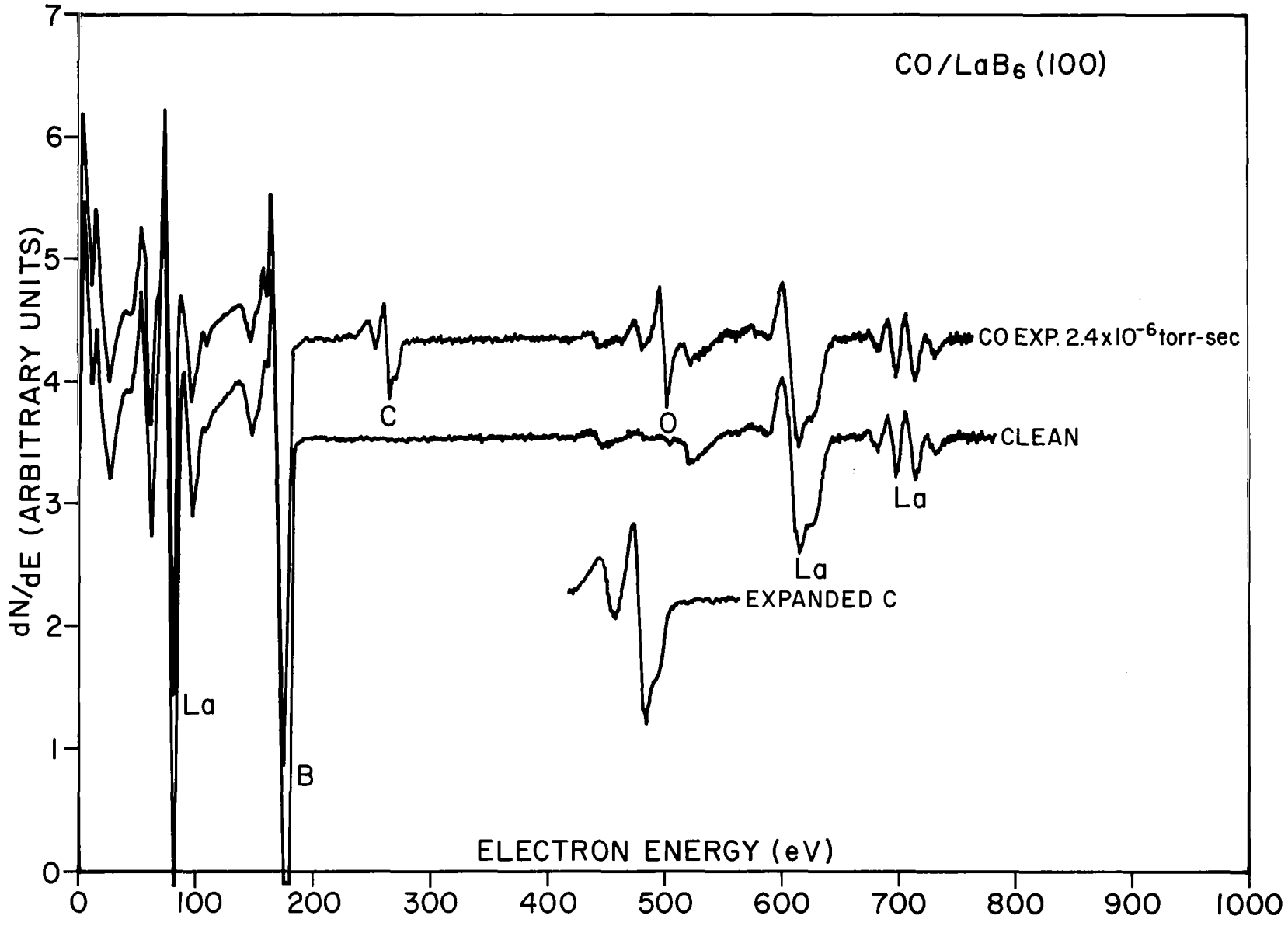

Figure 8 Auger derivative spectrum of a clean and CO covered LaB_6(100) crystal face using 2 V modulating voltage. Electron gun conditions: V = 4 kV and I = 10 μA.

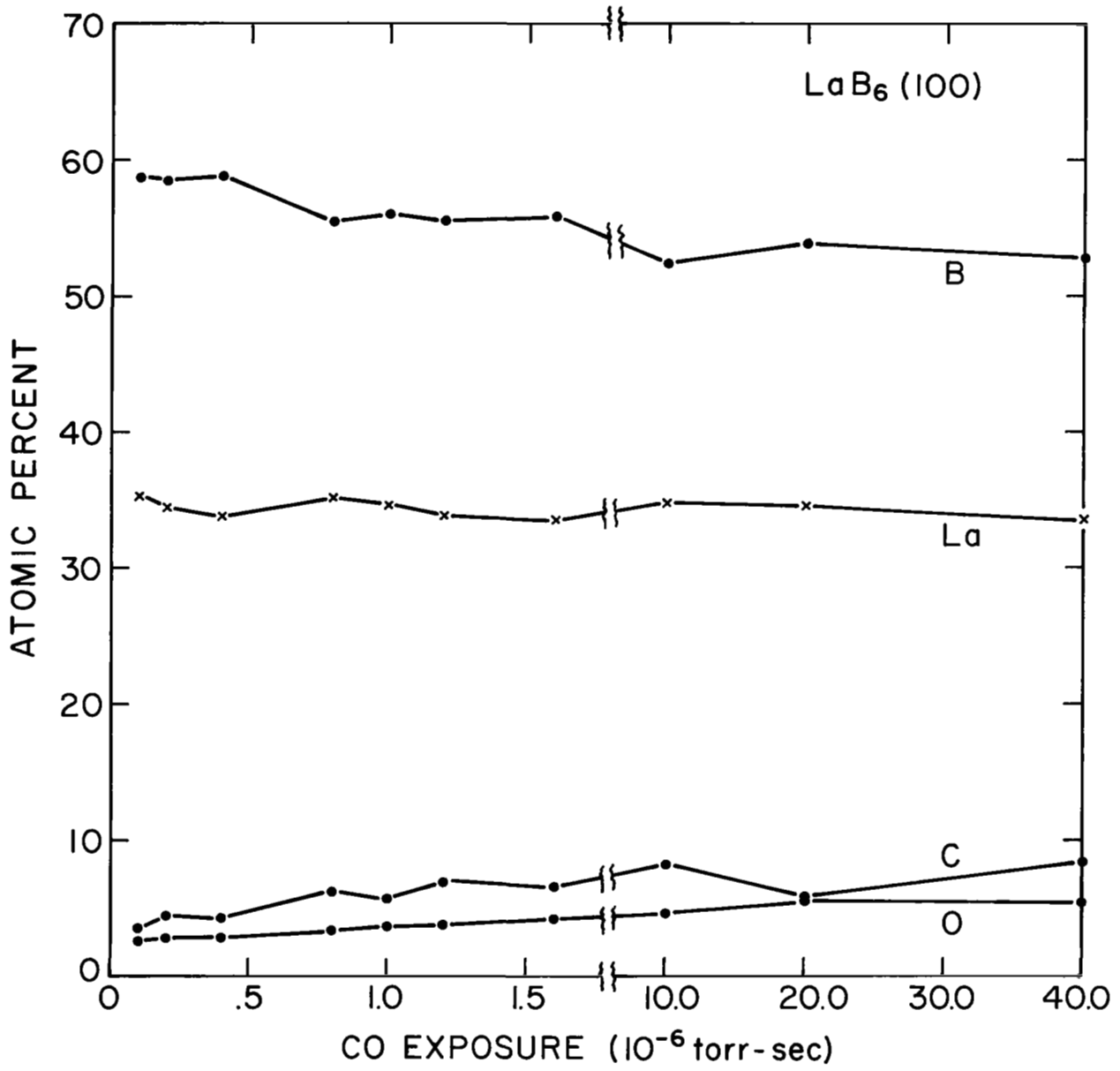

Figure 9 Curves show the variation of elemental composition of a LaB_6(100) crystal surface as determined by AES upon CO adsorption at 300 K. Table III Auger sensitivities were employed.

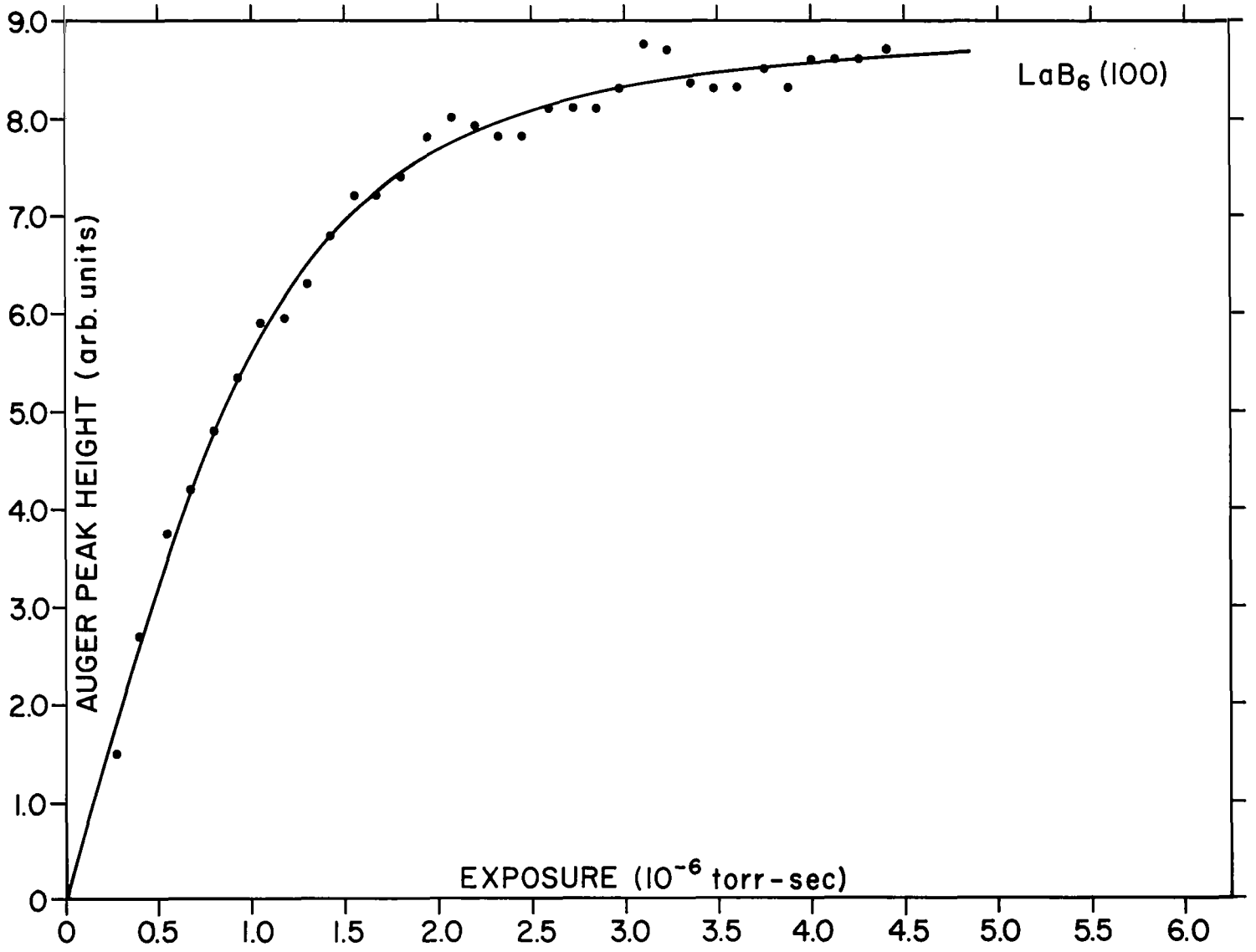

Figure 10 Curve shows the variation of the O (510) Auger signal strength with CO exposure for a LaB_6(100) crystal face at 300 K.

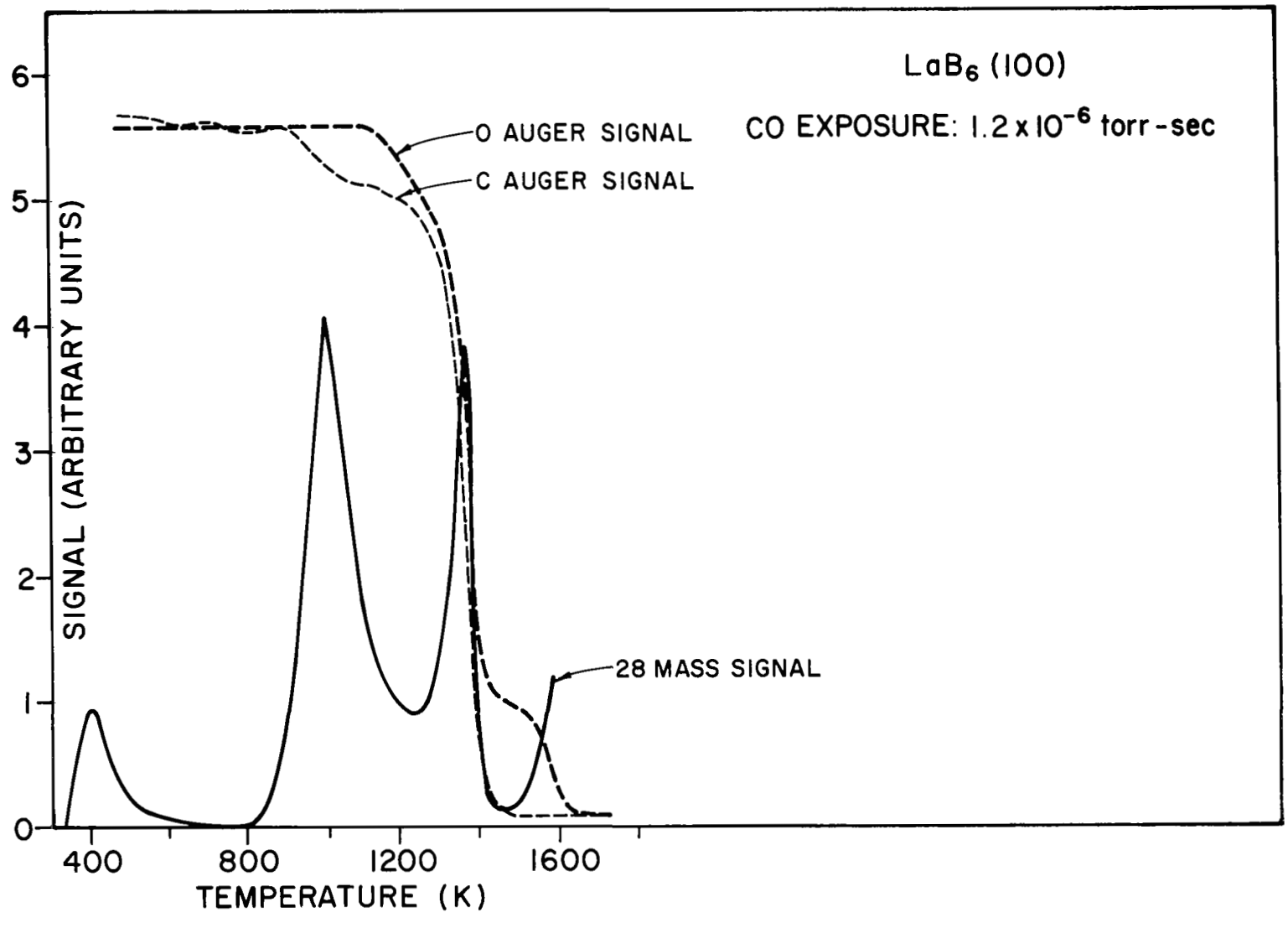

Figure 11 Curves show the variation of the O (510) and C (271) Auger and mass 28 signal strengths with increasing temperature of a CO covered LaB_6(100) crystal face. Adsorption was carried out at 300 K and the heating rate was 32 K/sec.

with the 1400K desorption peak, we conclude that this corresponds to the removal of CO. Although the C(271) Auger signal drops slightly at 1000K coincident with the 1000K 28 mass peak, our tentative conclusion is that this desorption peak is due to CO desorption from the carbon binder on the back side of the crystal.

A further study of the CO thermal desorption and work function effects on LaB_6 (100) will be carried out using a pure Re support structure. This will eliminate some of the ambiguity in the flash desorption spectra.

5. Clean Surface Work Function and Electron Emission

A smooth LaB_6 (100) platelet crystal with an area of 0.0256 cm^2 was used to measure the FERP work function and thermionic emission coefficients. Figure 12 shows the crystal current vs the emitter to collector voltage for two values of voltage V_m on the mesh electrode facing the collector. For V_m = 5 V only the elastically reflected electrons (or more correctly only the specularly reflected electrons) are returned to the mesh; thus the deviation of the experimental curve from the theoretical curve is a measure of the elastically reflected R_e electrons. On the other hand for V_m = 22 all reflected electrons are returned to the mesh. By subtracting R_e from the latter reflection coefficient a value of the inelastic reflection coefficient R_{in} is obtained.

Both R_e and R_{in} are plotted against primary electron energy E_p in Fig. 12. Of particular interest is the large value of R_e as E_p approaches zero.

According to the theory of the FERP technique[5] the onset of collector current or, more correctly, the value of the emitter-to-collector voltage 20 to 30 nV below the peak in the derivative curve shown in Fig. 13 is the collector work function. Thus, a room temperature work function of 2.28 $\pm$ .03 eV for LaB_6(100) is measured.

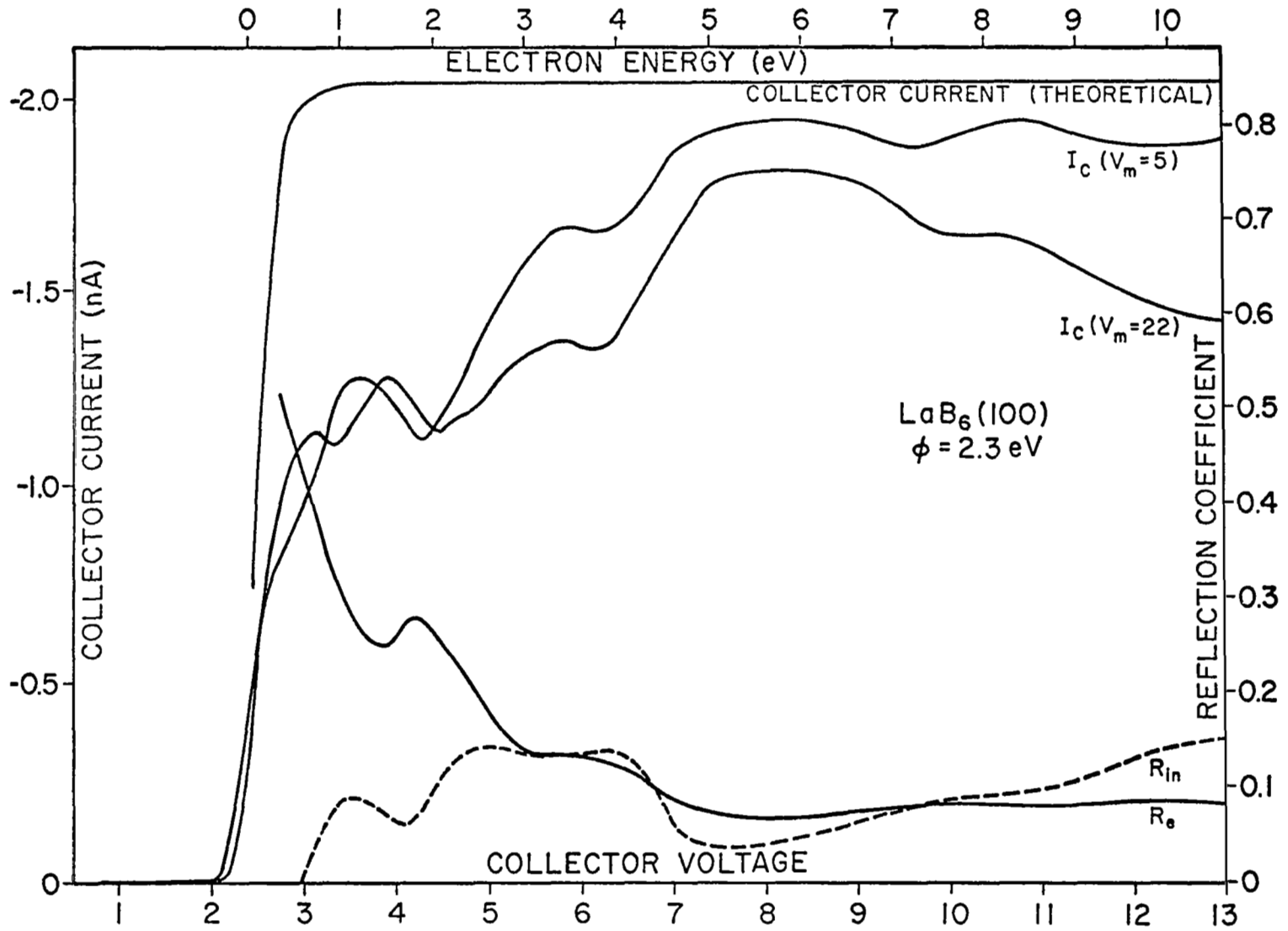

Figure 12. The theoretical and two experimental values of the collector current versus collector voltage for two values V_m of the mesh electrode facing the collector are given for an LaB_6 (100) collector crystal using the FERP technique.[5] Also given are the experimental values of the elastic R_e and inelastic R_{in} reflection coefficients as a function of primary electron beam voltage.

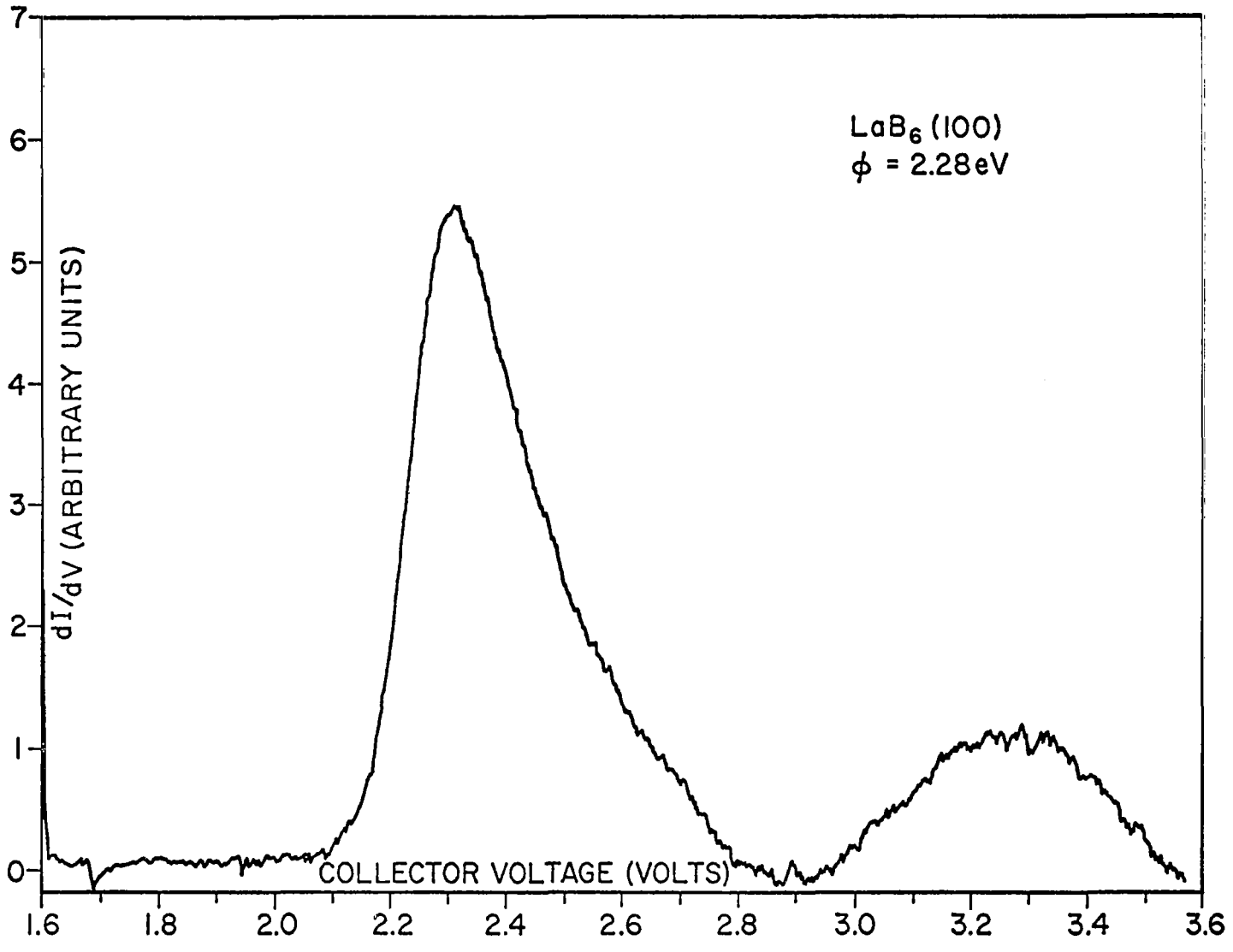

Figure 13. Curve shows the derivative of the V_m = 5 V retarding potential curve of Figure 12.

According to thermionic emission theory[7] the emitted current density J is given by the so-called Richardson equation:

$$J = (1-R)\ 120\ T^2 e^{-\phi/kT} \tag{1}$$

where R is the reflection coefficient at threshold. If an electric field $F = \beta V$ is applied to the emitter surface then

$$\phi = \phi_o - 3.8\ \beta^{1/2}\ V^{1/2} \tag{2}$$

where β is in Å^{-1} units. Thus a "Schottky" plot of ln J vs $V^{1/2}$ at constant T will allow extrapolation of the current to V = F = 0. In addition, should the work function have a linear temperature coefficient of the form

$$\phi(T) = \phi_o + \alpha T \tag{3}$$

then the Richardson equation becomes

$$J = (1-R)\ 120\ T^2 e^{\alpha/k}\ e^{-\phi_o/kT} \tag{4}$$

Thus, the deviation of the pre-exponential factor from 120 $A/cm^2\text{-}K^2$ is often taken as a measure of α in Eq. (3).

Schottky plots according to Eq. (2) were measured for a LaB_6 (100) clean crystal between 1400 and 1800 K. The results of the zero field emission current plotted according to Eq. (4) are given in Fig. 14 where $\phi_o = 2.47 \pm .05$ eV and $\alpha = 1.25 \times 10^{-4}$ eV/deg. As suggested by the Fig. 12 results a value of 1-R = 0.5 was used. Notice that J = 33 A/cm^2 at F = 0 and T = 2000 K.

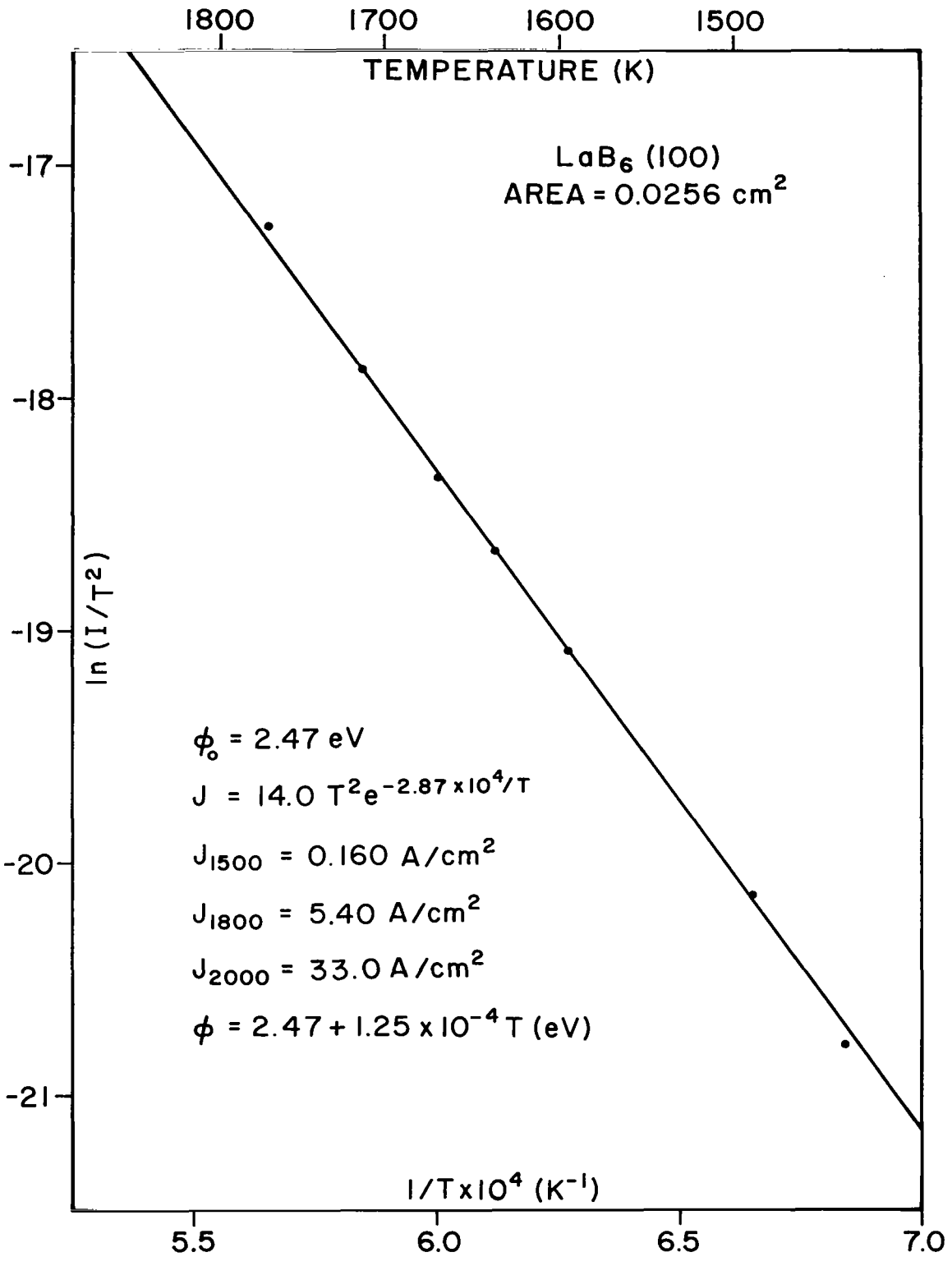

Figure 14 Curve shows a plot of the zero field emission current versus 1/T for a LaB_6(100) single crystal surface. The various emission coefficients are given.

IV. Cesiated LaB_6 (100) Surface Studies

A preliminary study of the effect and kinetic behavior of Cs on LaB_6 (100) has been carried out. The Cs source consisted of a mixture of Si/Cs_2CrO_4 which, when heated, undergoes a chemical reaction to give free Cs. We found it difficult to remove all traces of CO from this source and plan to employ a different source in future work. A further complication is that Cs is apparently very mobile on LaB_6 at room temperature. Thus the carbon support film, which has a high affinity for Cs, tended to act as an infinite sink for the Cs adsorbed on the LaB_6 surface. This problem will be rectified by employing a pure Re support structure and liquid N_2 cooling capabilities for the specimen.

Fig. 15 shows the Auger spectrum and the FERP derivative curve for a Cs coated LaB_6 (100) crystal. The surface is obviously contaminated with CO and we cannot be sure whether a substantial fraction of a monolayer of Cs exists on the surface. In spite of these problems we observed a work function lowering of 0.9 eV to ϕ = 1.39 eV.

Fig. 16 shows FERP data for the cesiated surface after the same fashion as given in Fig. 12 for the clean surface. Notice that the reflection coefficient at threshold is reduced somewhat from the clean surface.

Of considerable interest to thermionic converter use is the thermal desorption characteristics of Cs from LaB_6. To date only a small dose of Cs has been thermally flash desorbed from a relatively clean surface as shown in Fig. 17. This preliminary data suggests a relatively low binding energy of Cs to a clean LaB_6 (100) surface.

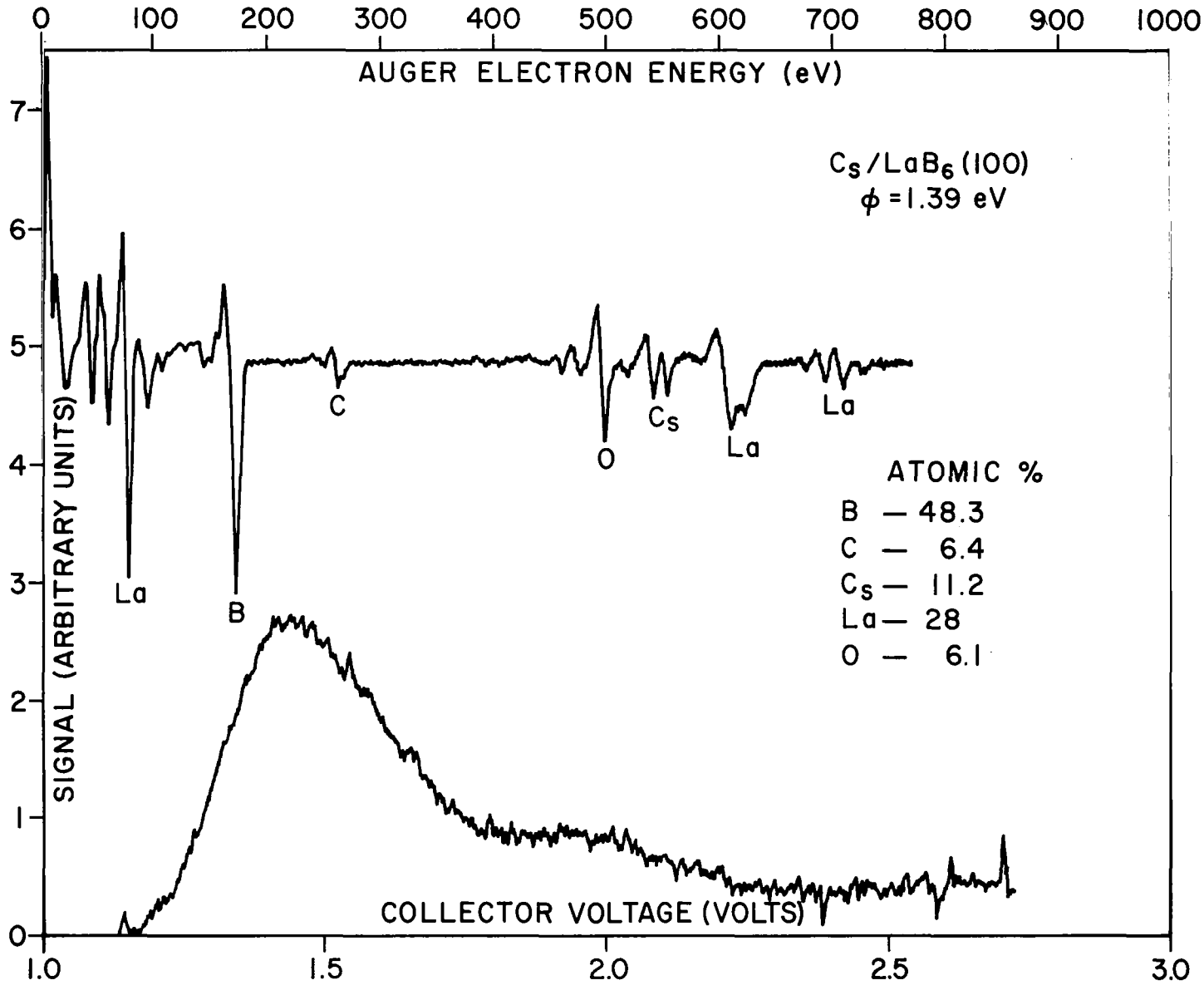

Figure 15 Upper curve shows the AES of a cesiated LaB_6(100) surface. Auger spectrometer settings are the same as in Figure 8. Lower curve shows the derivative FERP curved for the cesiated LaB_6(100) surface.

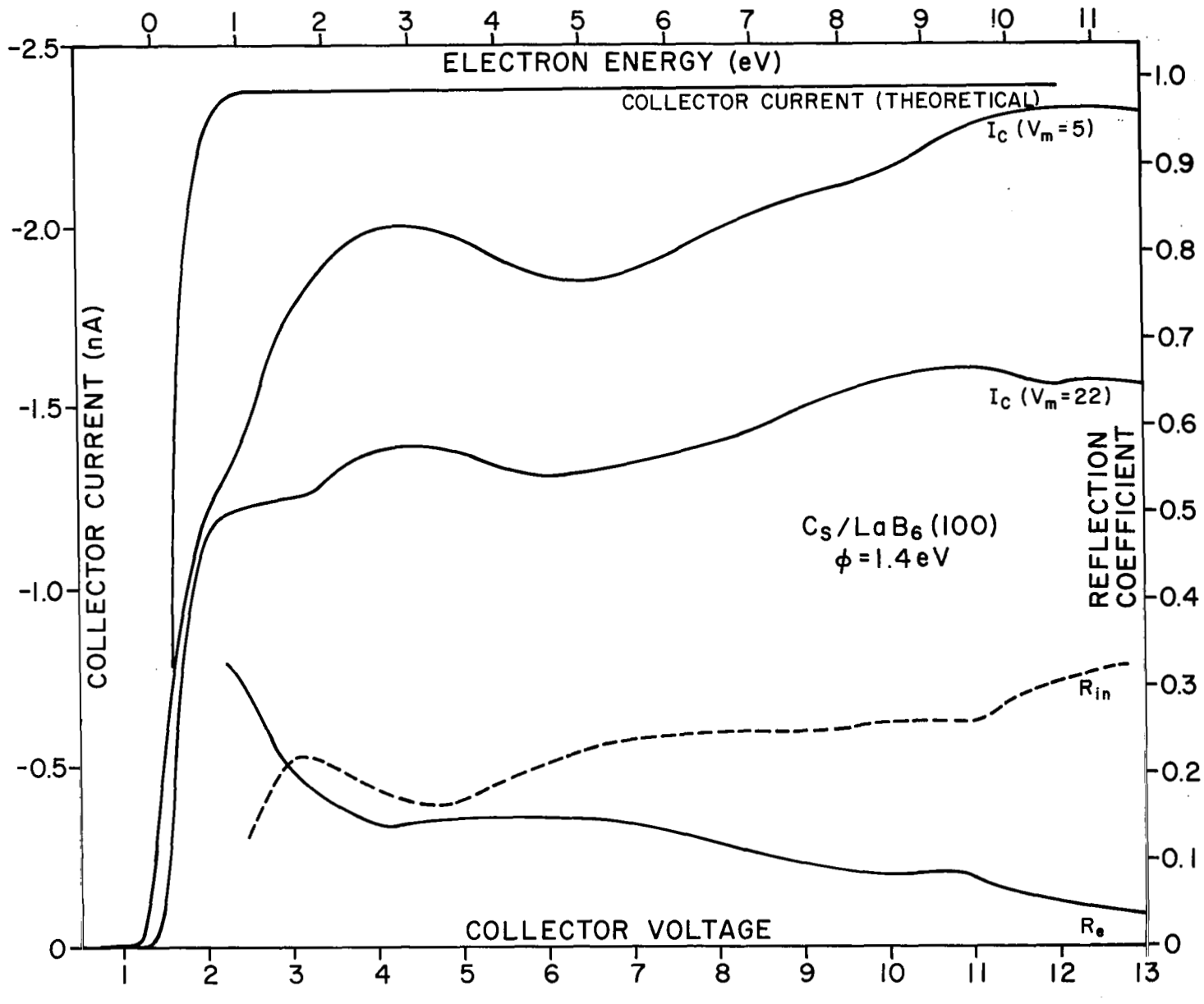

Figure 16 Same data as given in Figure 12 for a cesiated surface.

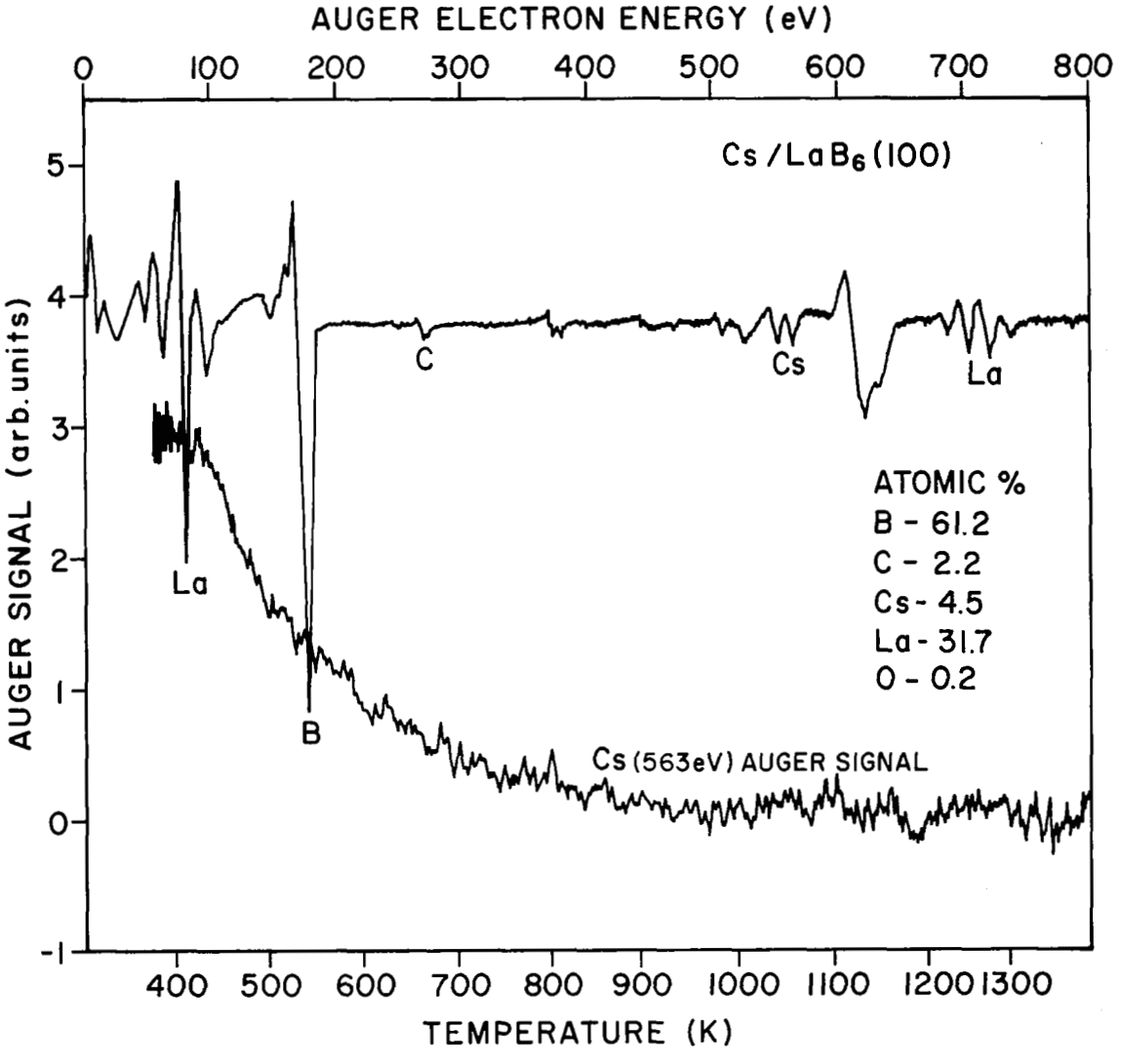

Figure 17 Upper curve shows the Auger spectrum of an initial dose of Cs that was subsequently thermally desorbed. Lower curve shows the diminution of the Ca (563 eV) Auger signal with temperature. The heating rate was 98 K/sec.

V. EVAPORATION CHARACTERISTICS OF LaB_6

An aspect of considerable discrepancy in the literature is the nature and stoichiometry of the evaporating species from pure LaB_6. For example, Lafferty,[8] Buckingham[9] and Oshima, et al,[10] using similar methods report an activation energy of desorption of 7.3, 3.25 and 4.1 eV respectively for the evaporating species believed by some[9,11] to be La. Other investigators,[10,11,12] making physical observations of the LaB_6 specimens and evaporation products, concluded that evaporation occurs with a near stoichiometric ratio of La/B. Recently, a stoichiometric ratio of atomic La and B in the vapor phase has been observed under equilibrium conditions.[13] The latter result is in general agreement with our mass spectrometric study of nonequilibrium evaporation which showed only atomic La and B in the vapor phase but with a ratio of B/La that varied from 6 to 3 over the temperature range 1700 to 2000 K.

Fig. 18 shows a typical plot of the log of the B^{10+} and B^{11+} mass spectrometer current versus 1/T for evaporation from a clean LaB_6 (100) crystal. Similarly in Fig. 19 a typical plot of the log of the La^{139+} current versus 1/T is shown. In order to evaluate the ratio La/B the variation of mass spectrometer sensitivity with mass number was first determined using H_2, Ne, Ar and Xe as calibrating gases. At the resolution setting employed in this study the transmission factor for La^{139}/B^{10} was 2.3×10^{-3}; in addition the electron impact ionization cross section coefficient ratio for $\sigma_{La}/\sigma_B = 5.66$ must be considered. Thus the La^+ current in Fig. 19 is normalized to the B^+ current level by multiplying by the aforementioned factors.

Also given in Fig. 19 is the B/La ratio variation with temperature. Within the uncertainties of the various correction factors and experimental errors, a stoichiometric ratio of B/La $\tilde{=}$ 6 is evident between 1700 and 2000K.

Table IV gives the activation energies of B and La desorption as obtained from the various runs which were plotted according to Figures 18 and 19.

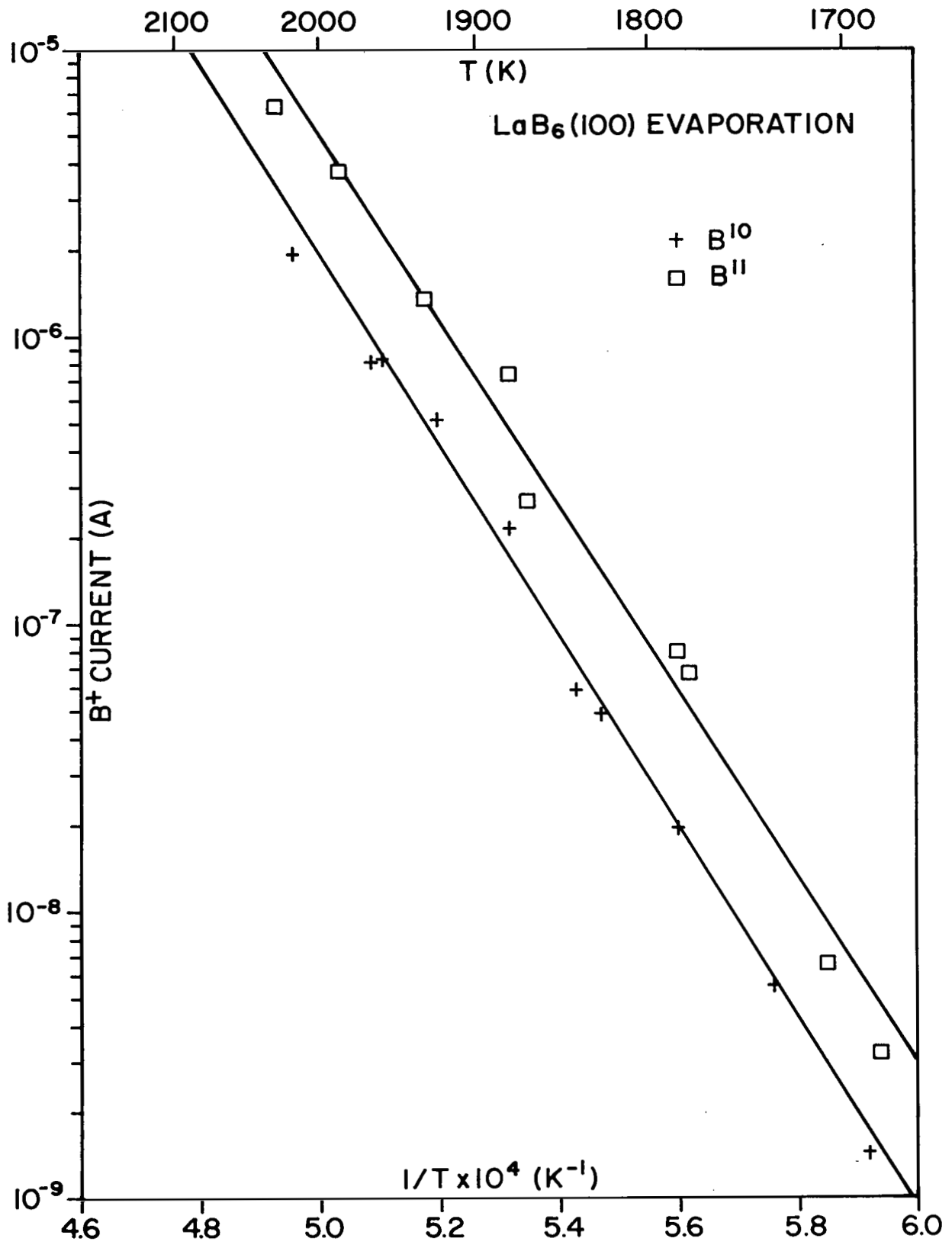

Figure 18 Plot of the mass spectrometer ion currents for the B^{10} and B^{11} isotopes evaporating from an LaB_6(100) crystal face as a function of temperature.

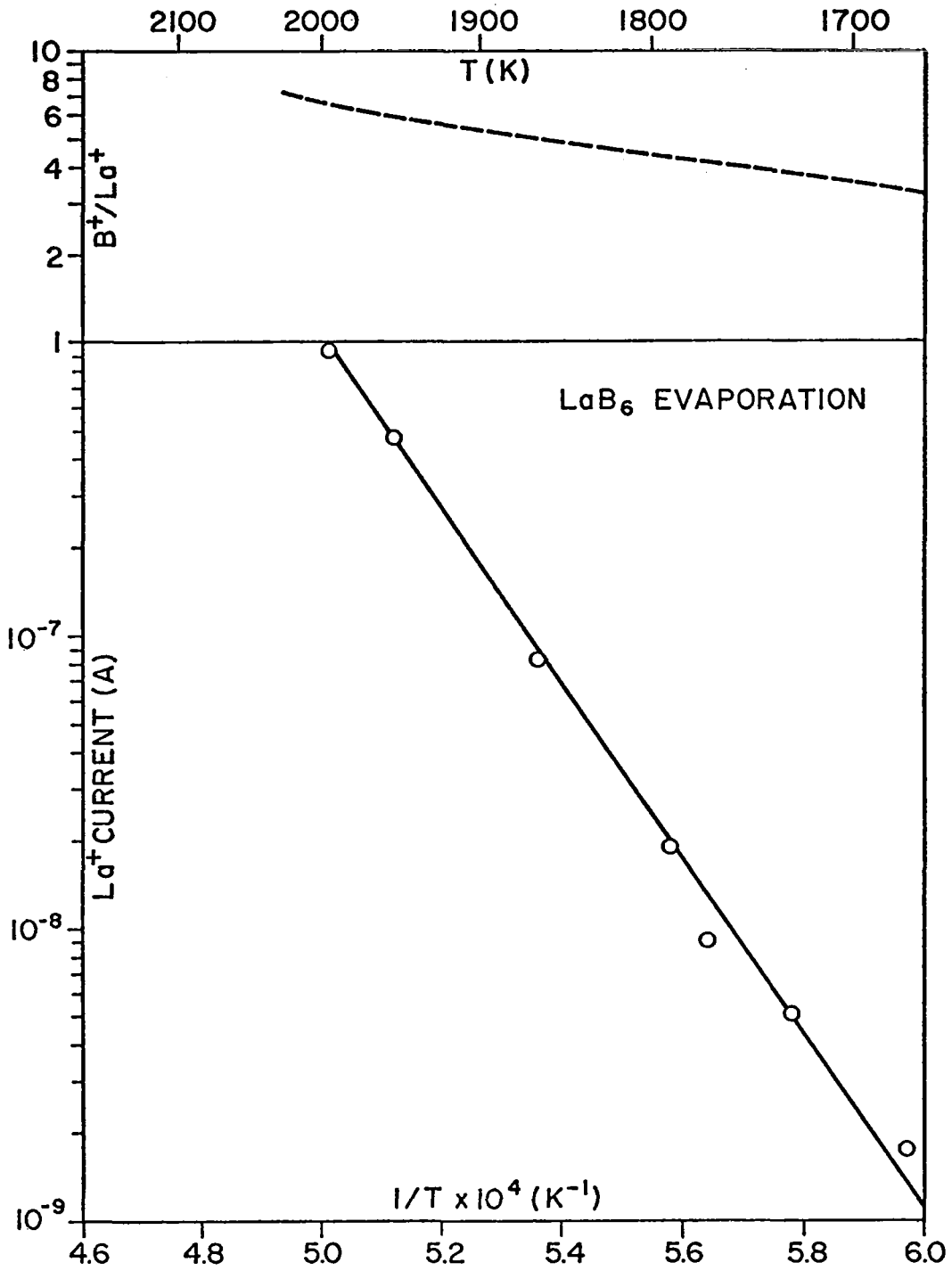

Figure 19. Plot of the mass spectrometric ion current for La^{139} evaporating from an LaB_6 (100) crystal face as a function of temperature. The La current values are normalized to the mass 10 transmission value of the mass spectrometer and are adjusted for the change in electron impact ionization cross section. At the top is given the approximate B/La ratio.

Within experimental error the activation energies for B and La are approximately the same. Ames[13] has obtained a value of 37 eV for the enthalpy of the reaction

$$LaB_6\,(s) = La\,(g) + 6B\,(g)$$

at 2275 K. As a crude approximation one may say that 1/6 of the enthalpy of the above reaction represents the La-B bond energy, i.e., 6.2 eV. The latter value, which represents the minimum value for the desorption energy of La or B from its surface, is in reasonable agreement with the Table IV values.

Table IV

Summary of the Desorption Activation Energies of La and B from a LaB_6 (100) Single Crystal Face

	Run I (eV)	Run II (eV)	Run III (eV)
La	7.1	5.8	6.1
B^{10}	7.0	6.6	-
B^{11}	7.0	6.4	-

$\overline{E}_{La} = 6.3 \pm 0.3$ eV

$\overline{E}_{B} = 6.8 \pm 0.3$ eV

Based on an extrapolation of Ames and McGrath's partial pressure data for B and La to lower temperature we give in Table V the partial pressure and approximate evaporation rate of LaB_6 at four temperatures. The last column in Table V gives the ratio of emission of electrons to evaporation of LaB_6 particles per unit area. The latter ratio can be considered as a figure of merit when the bare LaB_6 (100) crystal is compared with other thermionic emitters.

TABLE V

Partial Pressure and Evaporation Data for LaB_6

Based on Ames and McGrath's Data[13]

T (K)	P_{La} (torr)	P_B (torr)	Evap. Rate* (cm/sec)	N_e/N_{LaB_6} (electron/atom)
2000	3.1×10^{-4}	1.86×10^{-3}	2.9×10^{-6}	7.2×10^{2}
1800	1.2×10^{-5}	7.2×10^{-5}	1.2×10^{-7}	2.9×10^{3}
1600	2.1×10^{-7}	1.2×10^{-6}	2.2×10^{-9}	1.7×10^{4}
1400	1.1×10^{-9}	6.5×10^{-9}	1.2×10^{-11}	1.8×10^{5}

*Calculated from the Langmuir equation, flux = $P/(2\pi mkT)^{1/2}$, and a monolayer density and thickness of 4.1×10^{15} atoms/cm^2 and 4.15 Å respectively.

REFERENCES

1. J. F. Morris, "High Efficiency, Low Temperature Cesium Diodes with Lanthanum-hexaboride Electrodes," NASA TMX-71549.

2. B. Post, D. Moskowitz and F. W. Glaser, "Borides of Rare Earth Metals," J. Am. Chem. Soc. 78, 1800 (1956).

3. T. Aito, U. Kawabe and Y. Honda, "Single Crystal Lanthanum Hexaboride in Molten Aluminum," Japan J. Appl. Phys. 13, 391 (1974).

4. P. Lebeau and J. Eiguras, Compt. Rend. 127, 393 (1898).

5. R. W. Strayer, W. Mackie and L. W. Swanson, Surface Science 34, 225 (1973).

6. T. I. Serebrypkova, Yu. B. Paderno and G. V. Samsonov, Optika i Spektoros, 8, 410 (1960).

7. G. A. Haas and R. E. Thomas, Techniques of Metals Research, Part 1, Vol. VI, 91 (1972).

8. J. M. Lafferty, J. Appl. Phys. 22, 299 (1951).

9. J. D. Buckingham, Brit. J. Appl. Phys. 16, 1821 (1965).

10. C. Oshima, S. Horuichi and S. Kawai, Japan J. Appl. Phys., Suppl. 2, Part 1, 281 (1974).

11. H. Ahmed and A. N. Broers, J. Appl. Phys. 43, 2185 (1972).

12. R. R. Ford and D. Lichtman, J. Appl. Phys. 44, 4378 (1973).

13. L. McGrath, New Mexico State University Ph.D. Thesis, "Vaporization Thermodynamics of the Rare Earth Borides," Univ. Microfilm (1972) and L. L. Ames and L. McGrath, High Temp. Sci. 7, 44 (1975).

NASA-Langley, 1976 E-8624